Performance of steel reinforced concrete filled stainless steel tubular columns at elevated temperature

Qinghua Tan[1, 2*], Leroy Gardner[2] and Linhai Han[3]

[1] Department of Material Science and Engineering , National University of Defense Technology, P. R. China

[2] Department of Civil and Environmental Engineering, Imperial College London, UK

[3] Department of Civil Engineering, Tsinghua University, P. R. China

Abstract

Steel reinforced concrete filled stainless steel tubular (SRCFSST) columns combine the advantages of concrete filled stainless steel tubular (CFSST) columns and steel reinforced concrete (SRC) columns, resulting in excellent corrosion resistance, good economy, good ductility and excellent fire resistance. Thus, SRCFSST columns have many potential structural engineering applications, especially in offshore structures. The performance of SRCFSST columns at elevated temperature is investigated by finite element (FE) analysis in this paper. Firstly, FE models capable of capturing the full load-deformation response of structural members at elevated temperatures are developed and validated against relevant published tests on CFSST and SRC columns under fire conditions. Based on the validated FE models, the behavioural mechanisms of the SRCFSST columns under fire are explained by analysis of the sectional temperature distribution, typical failure modes, axial deformation versus time response and load redistribution. Finally, the fire resistance of SRCFSST columns is evaluated in comparison to CFSST columns with equivalent sectional load-bearing capacity at ambient temperature or equivalent steel ratios. The results lay the foundation for the development of fire resistance design rules for SRCFSST columns.

Keywords: Steel reinforced concrete filled stainless steel tubular (SRCFSST) column, Fire resistance, Finite element (FE) models, Fire safety engineering.

*Corresponding author. Tel.: +86 731 87007262, E-mail address: tanqinghua@nudt.edu.cn (Qinghua Tan)

1 Introduction

By replacing the outer carbon steel tube with a stainless steel tube, concrete-filled stainless steel tubular (CFSST) columns can combine the advantages of concrete-filled steel tubular columns (CFST) and stainless steel, resulting in greater corrosion resistance, enhanced ductility and improved fire resistance. However, as a result of the high initial cost of stainless steel, the initial cost of CFSST columns is higher than that of CFST columns for a given load-bearing capacity. Embedding carbon steel profiles inside a CFSST column forms the steel reinforced concrete filled stainless steel tubular (SRCFSST) column, which combines the advantages of CFSST columns and steel reinforced concrete (SRC) columns; typical cross-sections are shown in Fig. 1. Compared with CFSST columns, SRCFSST columns have lower initial cost due to the reduced amount of stainless steel, while the encased profile enhances the integrity, ductility and fire performance.

In the past ten years, there have been a number of research investigations into the static response, impact resistance and fire performance of CFSST columns. For the static performance, experimental and numerical studies have been conducted on CFSST stub columns without stiffeners [1-5], with stiffeners [6-8], and involving lean duplex stainless steel [9] and elliptical cross-sections [10, 11] under axial compression; CFSST columns subjected to combined axial compression and bending have been studied by Uy et al. [5]. The results show that CFSST columns generally have improved structural performance over conventional CFST columns and that existing design rules for CFST columns are somewhat conservative in predicting the load-carrying capacities of both stub and slender CFSST columns.

The impact resistance of CFSST members has been studied experimentally and numerically; lateral impact tests were performed on CFSST members restrained axially and rotationally at their ends, while the general impact behaviour was also investigated through finite element (FE) modelling [12-14]. The results showed that CFSST columns had improved strength and ductility compared with their CFST counterparts.

For fire performance, Han et al. [15] tested five axially-loaded CFSST columns at elevated temperature, where austenitic stainless steel was used for the outer tubes. The test parameters included section type (circular or square), load level (0.15-0.45) and cross-section dimension (300-630 mm). FE models were then validated against the test results, and a parametric analysis was conducted to investigate the key factors affecting the fire resistance of CFSST columns. The parametric analysis showed that the section type, section size, slenderness ratio and load level are critical parameters. Finally, two design tables were proposed to predict the fire resistance of CFSST columns under standard fire conditions. Tao and Ghannam [16] employed FE modelling to determine the temperature field in CFST and CFSST columns. A comparison between the two types of columns revealed slower temperature development in the CFSST columns as a result of the lower thermal conductivity and emissivity of stainless steel. Tao et al. [17] carried out an experimental and analytical investigation of CFSST columns in fire and after fire exposure. A total of 12 specimens were tested, including 6 CFSST columns in fire, while the remaining 6 CFSST columns were subjected to sequential ambient temperature loading, fire exposure including both heating and cooling phases under constant applied load and post-fire loading phases. A photogrammetric method was employed prior to and during the tests to capture the initial imperfections of the CFSST columns and the development of strain in the stainless steel tubes in fire. An FE model was also established and shown to be able to replicate the experimental results with reasonable accuracy.

Overall, CFSST columns have been shown to offer improved static, fire and impact performance over CFST columns due to the greater ductility and favourable thermal characteristics of stainless steel. Similarly, SRCFSST columns are expected to show excellent ductility and fire performance. However, the fire performance of SRCFSST columns has yet to be investigated. In this paper, the performance of SRCFSST columns at elevated temperature is studied by means of numerical analysis. Firstly, FE models for composite columns at elevated temperature are established and validated on the basis of relevant published experimental data on CFSST and SRC columns under

fire. Based on the validated FE models, the behavioural mechanisms of SRCFSST columns under fire are explained by analysis of the typical failure modes and axial deformation versus time curves. Next, the internal redistribution of forces and the interaction between each component during the full-range elevated temperature and loading histories are explored. Finally, the fire resistance of SRCFSST columns is studied parametrically considering equivalent sectional load-bearing capacity at ambient temperature or equivalent steel ratios and assessed in comparison with that of corresponding CFSST columns.

2 Finite element modelling

Finite element models of SRCFSST columns in fire are developed and validated in this section. Since there are no published test data for the fire performance of SRCFSST columns, tests on CFSST and SRC columns under fire are used to validate the FE models indirectly.

2.1 Finite element models

The finite element package ABAQUS [18] is used to establish the FE models, which include calculation of the temperature field and sequential thermal-stress analysis. Descriptions of the adopted thermal and mechanical properties of the modelled stainless steel, carbon steel and concrete at elevated temperature, the approach taken to simulate the steel-concrete interface, the chosen element type and other modelling aspects are introduced below.

2.1.1 Temperature field analysis

An accurate representation of the thermal properties of the carbon steel, stainless steel and concrete, including the thermal conductivity, specific heat and thermal expansion are key to the precise prediction of the temperature field. Moreover, the contact conductance of the tube and concrete interface, convective heat transfer coefficient and emissivity of the surface exposed to fire and the effect of water evaporation are also important. Tao and Ghannam [16] and Han et al. [15] developed an FE model to predict the temperature field in CFSST columns, and comparisons were conducted to

validate the models against the relevant temperature data recorded in the tests. Based on the findings of the above research, the thermal properties of concrete and reinforcement set out in EN 1992-1-2 [19], and those of stainless steel and carbon steel provided in EN 1993-1-2 [20], respectively, are employed herein. For the convective coefficient and emissivity of the surfaces exposed to fire, 35 ($Wm^{-2}K^{-1}$) and 0.2 for stainless steel proposed by Gardner and Ng [21], and 25 ($Wm^{-2}K^{-1}$) and 0.7 for carbon steel as given in EN 1993-1-2 [20], are used respectively. The contact conductance of the tube and concrete interface for CFSST columns reported by Han et al. [15] and CFST columns reported by Ghojel [22] are adopted. For the effect of water evaporation, a simple and practical method of increasing the specific heat of concrete between 100 and 200 ℃ according to the moisture content in EN 1992-1-2 [19] is adopted, though, in generally, sensitivity analysis on moisture content for different tests is advised.

2.1.2 Structural analysis

(1) Material properties

The elastic modulus, thermal expansion coefficient and stress-strain models set out for stainless steel and carbon steel in EN 1993-1-2 [20] and reinforcement in EN 1992-1-2 [19] are adopted herein to describe their constitutive behaviour at high temperatures. The Poisson's ratios of stainless steel and carbon steel keep unchanged at elevated temperature and are set to 0.3. In these models, the effects of creep at elevated temperature have been implicitly included.

The concrete damaged plasticity model defined in ABAQUS [18] is used in the analysis, which defines the yield surface and the plastic behaviour based on the equivalent uniaxial stress-strain relationships of concrete. The compressive stress-strain relationship for confined concrete during the heating phase employs the model proposed by Song et al. [23], which was used in the FE analysis of CFSST columns under fire carried out by Han et al. [15] where good agreement between test and predicted results was obtained. The elastic modulus of confined concrete was obtained by the slopes

of original point and point with 0.4 times peak strength in the stress-strain curves at high temperatures.

For the tensile behaviour of concrete, the fracture energy criterion is adopted in this paper. The models for the influence of temperature on the fracture energy proposed by Zhang and Bicanic [24] and the tensile strength of concrete recommended in EN 1992-1-2 [19] are also used. The tensile strength is assumed to be 10% of the compressive strength $f_c^{'}$ at ambient temperature. The model of Poisson's ratio for concrete proposed by Izzuddin et al. [25] is used herein, which shows that the Poisson's ratio for concrete remains at 0.2 unchanged until 150 ℃, reduces to half of its ambient value at 400 ℃ and decrease to zero at 1200 ℃.

(2) Interface

In steel-concrete composite structures, steel and concrete interact by bond and slip. The surface-to-surface contact feature in ABAQUS [18] is adopted to simulate the interaction between the stainless steel or carbon steel tube and the in-filled concrete. "Hard contact" in the normal direction and Coulomb friction in the tangential direction are defined at the contact surfaces. For the Coulomb friction model, a friction coefficient of 0.25 is adopted for both the stainless steel and carbon steel tube. For columns with reinforcing bars or an embedded steel profile, the "embedded region" constraint is used based on the assumption that there is no relative slip between the reinforcing bars or steel profile and the concrete.

(3) Meshing and boundary conditions

Meshing and boundary conditions of the FE models for SRCFSST column are shown in Fig. 2. The same element meshing is used in both the temperature field and stress analysis models. A maximum element length of 20 mm is set following a sensitivity analysis of the meshing dimension. Solid elements are used for the in-filled concrete, shell elements are used for the stainless steel or carbon steel tube and steel profile, and truss elements are used for the reinforcing bars. In order to simplify the analysis, the loading plates at the ends are modelled with a very high Young's modulus to ensure

that they remain essentially un-deformed during the loading process; meanwhile, two reference points, one at each end of the composite columns, are defined at the centroids of the loading plates with the "continuum distribution coupling" constraint applied between the loading plate and the corresponding reference point. The boundary conditions are applied to the FE model by assigning translational and rotational constraints directly on the reference points. The geometric imperfection of the columns is specified to take the shape of the first global buckling mode, with its maximum amplitude being the measured value in the test when available, or $H/2000$ (H is the height of column) according to Han et al. [15] (2013) and Gardner and Ng [21] when the imperfection of the tested column was not measured.

2.2 Validation of FE models

To validate the FE models, relevant test data for CFSST columns in fire reported by Han et al. [15] and Tao et al. [17], and SRC columns subjected to the ISO-834 standard fire [26] reported by Han et al. [27] are utilized since there are no published data for SRCFSST members under fire. For CFSST columns, Han et al. [15] tested five axially-loaded specimens in fire, while Tao et al. [17] tested 12 specimens in fire and after fire, but only the six in fire are used in this paper. For SRC columns, four specimens with H-shaped and cross-shaped embedded steel profiles subjected to the ISO-834 standard fire [26] were experimentally investigated by Han et al. [27]. The test results, including temperature-time curves, axial deformation development, failure modes and fire resistance, are compared with the corresponding FE predicted results obtained herein.

Fig. 3 shows typical observed and predicted column failure modes. It was found that the tested specimens behaved in a relatively ductile manner until the load applied by the axial hydraulic jack on the column could no longer be maintained. The failure mode of the columns is related closely to the section type and boundary conditions of the columns. The CFSST pin-ended columns tested by Han et al. [15] showed compression failure modes under non-ideal pinned boundary conditions as a result of possible restraint from rigid blocks bearing against the spherical hinges. For the square

specimens, no obvious lateral deformations occurred in the tests and this was mirrored in the simulations; evenly distributed local buckling waves were observed along the member length. For the circular specimens, small lateral deflections and local buckling, which occurred at the mid-height, were observed both in the tests and in the simulations. The pin-ended CFSST columns tested by Tao et al. [17] showed compressive and flexural failure modes. The circular columns generally failed due to overall buckling accompanied by local buckling of the steel tube near the mid-height of the member, while the square columns developed almost evenly distributed local buckling along the length of the steel tube. The SRC columns with pinned-fixed boundary conditions tested by Han et al. [27] showed compressive and flexural failure modes both in the tests and FE simulations, in which parallel and diagonal cracks were observed in the tension zone at mid-height, and concrete spalling was also observed in the compressive zone.

Fig. 4 shows a comparison of the predicted and tested fire resistances which are the elapsed time for which the test specimen continues to maintain its ability to support the test load under the standard fire, for example, the ISO 834 standard fire [26]. Generally, the predicted results are acceptable. The maximum disparities between the predicted and tested results are around 10%, and the predicted divided by test fire resistances have a mean ratio of 1.048 and a COV of 0.071. From the above comparisons, it can be concluded that, in general, the accuracy of the FE simulations is good, and that the modelling can now be extended to perform mechanical analysis of SRCFSST columns under fire conditions.

3 Full-range analysis of structural deformations

In this section, the behaviour of a typical SRCFSST columns is examined to explore the general response of this cross-section type in fire. The SRCFSST columns modelled in this section are based on a CFST column used in a practical engineering application in China [28]; the SRCFSST column and the CFST column have equal load-bearing capacity, as described in Section 4.1. The considered composite SRCFSST column has a circular cross-section (788 mm × 10 mm) and a

height (H) of 6400 mm, marked as SRCFSST-LC-10 in Table 2. The other geometrical and mechanical parameters are described in Section 4.1 and Table 2.

The applied load ratio is 0.4, calculated as $n = N_F/N_u$, where N_F and N_u are the axial load applied to the column and the load-bearing capacity of the composite column at ambient temperature, respectively. N_u can be determined according to EN 1994-1-1: 2004 [29]. The composite column is heated evenly following the ISO 834 standard fire [26].

3.1 Temperature versus time curves

Temperature (T) versus time (t) curves for the modelled specimen are shown in Fig. 5. The following points are monitored: two interfacial points (point 1 at the inner surface of the stainless steel tube, and point 2 at the surface of the in-filled concrete), one point within the in-filled concrete (point 3 at the midpoint of the radius), and three points on the embedded steel profile (point 4 at the edge of the flange, point 5 at the midpoint of the flange and point 6 at the midpoint of web). For the interfacial temperature at points 1 and 2, as shown in Fig. 5(a), it can be seen that the temperatures at point 1 at the inner surface of the stainless steel tube are higher than at point 2 at the surface of the in-filled concrete, with a maximum difference of up to 248 °C, as a result of the inclusion of the heat conductance of the interface. For the concrete temperature at point 3 shown in Fig. 5(a), the temperatures remains below 110°C in the predicted curve due to the protection of the outer stainless steel tube and concrete layer. For the temperature of the embedded steel profile at points 4, 5 and 6, as shown in Fig. 5(b), the temperature of the embedded profile remains below 200 °C due to the protection of the stainless steel tube and surrounding concrete, which means that the steel profile maintains almost its full room temperature strength and bears a higher proportion of the load, transferred from the degraded concrete and stainless steel tube, at elevated temperatures.

Additionally, the predicted curves for points 2 and 3 in the concrete appear to have a plateau at 100 ～200 °C, which also occurred in the corresponding fire tests. The results shows that the increase in

the specific heat of the concrete between 100° C and 200 °C in the FE model can capture the characteristic of the water in the concrete evaporating at approximately 100°C.

3.2 Failure modes

The deformed shape of the studied SRCFSST column at failure in fire is shown in Fig. 6. The member fails with global lateral bending since the column is susceptible to global buckling (slenderness λ=32.5) and has an initial imperfection of amplitude H/2000. Significant local buckling is also observed in the compressive zone within a 800 mm length along the mid-height of the stainless steel tube while slight local buckling is observed within a 1100 mm length near both ends of the column, as shown in Fig. 6 (a). Significant global lateral bending is observed in the steel profile without obvious local buckling due to the restraint from the in-filled concrete, as shown in Fig. 6 (b). For stockier columns, not susceptible to global buckling, lateral bending would of course be substantially reduced. The observed failure mode of the SRCFSST columns at elevated temperature is similar to that of CFSST columns reported in Han et al. [15] and Tao et al. [17], but the former can endure longer fire exposure times than the latter.

3.3 Axial deformation versus time curves

Fig. 7 shows the axial displacement of the loading plate (Δ) verses fire exposure time (t) curve of the considered SRCFSST column at elevated temperature. The typical Δ-t curves can be divided into four characteristic stages, i.e.

(1) Ambient loading stage (O-A). During this stage, the load applied to the SRCFSST column is increased linearly to the design load.

(2) Expansion stage (A-B). During this stage, the load on the SRCFSST column remains constant, and the environmental temperature increases following the ISO 834 standard fire curve [26]. With increasing temperature, the material expands and degrades simultaneously. However, in this stage, the axial deformation associated with thermal expansion is dominant over that due to material degradation. Therefore, the column expands until the effects of material expansion and degradation

are balanced. The balance point is marked as point B in Fig. 7 where the expansion displacement reaches its peak value and the expansion stage ends.

(3) Creep stage (B-C). During this stage, the applied load is still kept constant and the temperature is increased further following the ISO 834 standard fire curve [26]. As the material temperature increases, the contractive deformation due to the material degradation under high temperature becomes dominant. The total axial deformation of the column changes from expansion to contraction. The contraction increases gradually as the material is heated and deteriorates further, while the lateral deflection of the column also starts to rise. The softening stage ends at point C.

(4) Accelerated failure stage (C-D). In this stage, the second-order effect induced by the axial force and the lateral deformation becomes dominant; as a result, the axial deformation of the column increases sharply and the column fails when the maximum axial contraction or the rate of contraction reach the failure criteria specified in ISO-834-1 [26].

When the load ratio of the column exceeds 0.4, the axial expansion becomes very small, even non-existent in SRCFSST columns because the contractive deformation induced by the axial load and material degradation dominate over the effect of thermal expansion. For example, when the load ratio of the column is 0.6, the Δ-t curve only contains three stages, i.e. the ambient loading stage (O-A'), the creep stage (A'-C') and the accelerated failure stage (C'-D') in Fig. 7.

3.4 Load redistribution

An SRCFSST column is composed of an outer stainless steel tube, in-filled concrete and an embedded carbon steel profile, and the external load is borne by the three components. At ambient temperature, the loads are borne by the three parts according to their axial stiffness. However, in fire, the properties of the constituent material degrade as the temperature rises, and the relative axial stiffness of the constituent components change. Therefore, for a constant external load, the section internal forces of an SRCFSST column redistribute among the three components as the environment temperature increases. To examine the internal force redistribution in SRCFSST columns during the

ambient temperature and heating phases, the proportions of the applied load carried by the stainless steel tube (p_t), the in-filled concrete (p_c) and the carbon steel profile (p_p) are extracted from the FE analysis, and the proportion versus time curves are shown in Fig. 8, in which points O, A, B, C and D correspond to the key points in Fig. 7. Positive and negative values of the proportion represent the specified part being in compression and tension, respectively. It can be seen from Fig. 8 that:

(1) Ambient loading stage (O-A): All three components of the SRCFSST column are in compression at the end of the ambient temperature phase (point A), in which, p_t =18.7%, p_c =56.7% and p_p =24.6% for the considered cross-section.

(2) Expansive and creep stage (A-B-C): At the beginning of the heating phase, the stainless steel and the outer layer of concrete are heated and their properties degrade; the corresponding loss of axial stiffness causes load to be transferred to the embedded steel profile. It is shown in Fig. 8 that p_t and p_c decrease while p_p increases until it reaches the peak value p_p=65.7% (corresponding to p_t =7.8% and p_c =26.5%). As the heating time increases, the temperature of the inner material layers including the concrete and the embedded steel profile increases, and the proportion of the load borne by the steel profile p_p reduces from 65.7% to 50.2%, while the proportion of the load borne by the outer tube p_t decreases further from 7.8% to 2.1%.

(3) Accelerated failure stage (C-D): As the temperature increases further, the proportion of the load borne by the outer tube reduces from 2.1% to 2.0%, and the corresponding value of p_p drops to 49%.

In general, the proportion of the load borne by the outer tube p_t continues to decrease during the entire heating time from 18.7% to 2.0%, while the embedded steel profile, which is thermally protected by the concrete, generally plays an increasingly important role in bearing the applied load throughout the fire exposure with p_p varying between 24.6% and 65.7%.

4 Comparisons of fire resistance of composite columns

4.1 Description of specimens for parametric analysis

In order to access and optimize the fire performance of SRCFSST columns as well as to quantify the advantages of SRCFSST columns over CFSST and CFST columns, parametric analyses and comparisons are conducted. A CFST section of 800 mm diameter and 16.0 mm thickness, used in a practical engineering application in China [28] was chosen as a reference section for comparing the different composite configurations; the height (H) of the CFST column was 6400 mm.

Two different series of numerical simulations were conducted in the parametric study. In Series 1, all the columns had the same steel ratio and diameter of in-filled concrete, i.e., the same total cross-sectional area of steel was split between the outer stainless steel tube and the embedded inner carbon steel profile. The examined composite columns in Series 1 are listed in Table 1. In Series 2, all the columns had the same axial load-bearing capacity at room temperature, as shown in Table 2.

The cube strength and elastic modulus of the in-filled concrete were taken as 60 MPa and 3.6×10^4 N/mm^2, respectively. For the CFSST and SRCFSST columns, the outer tube was formed from Grade S304 austenitic stainless steel, which is specified in CECS 410: 2015 [30] to have a 0.2% proof strength ($\sigma_{0.2}$) and ultimate strength (σ_u) of 205 MPa and 515 MPa, respectively. The yield stress and elastic modulus of the embedded H-shaped carbon steel profile, and the outer tube for the composite CFST sections, were taken as 345 MPa and 2.05×10^5 N/mm^2, respectively.

For comparison purposes, all the columns had a height (H) of 6400 mm with pinned-pinned boundary conditions at the two ends. The load ratio n was kept 0.4, and the composite columns were heated evenly following the ISO 834 standard fire [26]. The two series of columns were analyzed using the previously verified FE models.

4.2 Comparisons between the composite columns with the same steel ratio

The axial load-bearing capacity at ambient temperature and fire resistance of the composite columns in Series 1, as determined from the FE models, are listed in Table 1, where A_c, A_{sc}, A_{sp} and A_{ss} are the area of the in-filled concrete, the outer carbon steel tube, the embedded carbon steel profile and the outer stainless steel tube, respectively. As can be seen, the reference CFST column has the maximum axial load-bearing capacity at ambient temperature, but a very limited fire resistance of only 41.5 min; replacing the outer carbon steel section with a stainless steel section (CFSST-SR-16), the axial load-bearing capacity at ambient temperature is less than the reference column since the yield strength of the chosen stainless steel is less than that of the chosen carbon steel. However, the CFSST column extends the fire resistance by as much as 56% over the reference CFST column.

When the split between the steel areas is varied, it is found that decreasing the area of the outer stainless steel tube (A_{ss}) and increasing the area of the embedded carbon steel section (A_{sp}) means the relative ratio of cross-sectional areas of the two steel parts (A_{sp}/A_{ss}) increasing; the axial load-bearing capacity at ambient temperature and the fire resistance firstly increase and then decrease, with an optimal response achieved around Specimen SRCFSST-SR-8 with the A_{sp}/A_{ss} of 1.02. This is because as the thickness of the outer tube decreases, the tube becomes more susceptible to local buckling and the confinement from the tube to the concrete weakens. In fact, the ratio of the diameter-to-thickness of the outer tube for Specimen SRCFSST-SR-6 is 130, which is greater than the maximum value of 103 prescribed in EN 1994-1-1-2004 [29] for circular hollow steel sections. The fire resistance of Specimen SRCFSST-SR-8 is about 2.5 and 1.6 times as those of the CFST and CFSST columns with the same steel ratio.

It is therefore shown that SRCFSST columns offer a good solution for enhancing the fire resistance of traditional CFST or CFSST columns, but the cross-sectional areas of the outer tube and inner steel profile should be chosen carefully to find the optimal balance between ambient temperature

performance and fire resistance. Similar conclusions were reached by Espinos et al. [31] for traditional CFST columns with embedded HEB profiles.

4.3 Comparisons between the composite columns with the same load-bearing capacity

In Series 2, the studied composite columns have the same axial load-bearing capacity at ambient temperature; the steel ratio and fire resistance of these are listed in Table 2. As can be seen, the reference CFST column has a very limited fire resistance of only 41.5 min; replacing the outer carbon steel tube with stainless steel (Specimen CFSST-LC-24) requires the steel ratio of the CFSST column to be increased by 4.44% to maintain the same ambient load-bearing capacity due to the lower yield strength of the stainless steel. However, the CFSST column extends the fire resistance by as much as 58% over the reference CFST column. Additionally, the fire resistance of Specimen CFSST-LC-24 is only marginally higher than that of Specimen CFSST-SR-16 in Table 1, which shows that only increasing the thickness of the outer stainless steel tube does not significantly enhance the fire resistance of CFSST columns.

Maintaining a constant axial load-bearing capacity at ambient temperature and decreasing the area of stainless steel tube means increasing the area of the embedded carbon steel profile, and generally decreasing the steel ratio of the SRCFSST columns due to the lower yield strength of the chosen stainless steel, while the relative ratio of cross-sectional areas of the two steel parts (A_{sp}/A_{ss}) increases. The fire resistance shows firstly an increasing and then a decreasing trend when the area of the outer tube is reduced with the optimal performance arising around Specimen SRCFSST-LC-8 with the A_{sp}/A_{ss} of 1.73. The fire resistance of Specimen SRCFSST-SR-8 is about 6.9 and 4.3 times those of the CFST and CFSST columns with the same steel ratios. Since the outer stainless steel tube of Specimen SRCFSST-SR-6 is very thin-walled, severe local buckling of the outer tube occurs, prior to yielding of the inner steel profile under fire and the specimen fails at a fire exposure time of 71.9 min.

Therefore, when axial load-bearing capacity at ambient temperature is maintained, different factors including steel ratio, fire resistance and cost, should be considered in seeking the optimal SRCFSST solution.

5 Conclusions

Based on the results of this study, the following conclusions can be drawn:

(1) An FE model was developed to simulate the behaviour of SRCFSST columns at elevated temperature. The accuracy of this model was shown to be acceptable following comparisons with existing relevant test data.

(2) Based on the validated FE model, an SRCFSST column subjected to the ISO 834 standard fire curve was simulated and analysed. It was found that for the studied SRCFSST column, the outer stainless steel tube and the contact conductance of the interface delays the process of the heat transfer to the concrete and the inner steel profile, and the encased profile plays an important role in enhancing the fire resistance of the SRCFSST column.

(3) The relative cross-sectional areas of the two steel parts—the outer tube and inner steel profile of SRCFSST columns need to be carefully chosen to find the optimal balance between room temperature and fire performance.

Acknowledgments

The research reported in the paper is part of the Projects supported by the National Natural Science Foundation of China (No. 51308539) and the Natural Science Foundation of Hunan Province, China (No. 2018JJ2470). The financial support is highly appreciated.

References

[1] B. Young and E. Ellobody, Experimental investigation of concrete-filled cold-formed high strength stainless steel tube columns, *Journal of Constructional Steel Research*, 62(2006) 484-492.

[2] E. Ellobody and B. Young, Design and behaviour of concrete-filled cold-formed stainless steel tube columns, *Engineering Structures*, 28 (2006) 716-728.

[3] D. Lam and L. Gardner, Structural design of stainless steel concrete filled columns, *Journal of Constructional Steel Research*, 64 (2008) 1275-1282.

[4] Z. Tao, B. Uy, F. Y. Liao and L. H. Han, Nonlinear analysis of concrete-filled square stainless steel stub columns under axial compression, *Journal of Constructional Steel Research*, 67 (2011) 1719-1732.

[5] B. Uy, Z. Tao and L. H. Han, Behaviour of short and slender concrete-filled stainless steel tubular columns, *Journal of Constructional Steel Research*, 67 (2011) 360-378.

[6] E. Ellobody, Nonlinear behaviour of concrete-filled stainless steel stiffened slender tube columns, *Thin-Walled Structures*, 45(2007) 259-273.

[7] M. A. Dabaon, M. H. El-Boghdadi and M. F. Hassanein, Experimental investigation on concrete-filled stainless steel stiffened tubular stub columns, *Engineering Structures*, 31 (2009) 300-307.

[8] M. A. Dabaon, S. El-Khoriby, M. H. El-Boghdadi and M. F. Hassanein, Confinement effect of stiffened and unstiffened concrete-filled stainless steel tubular stub columns, *Journal of Constructional Steel Research*, 65 (2009) 1846-1854.

[9] M. F. Hassanein, Numerical modelling of concrete-filled lean duplex slender stainless steel tubular stub columns, *Journal of Constructional Steel Research*, 66 (2010) 1057-1068.

[10] X. Dai and D. Lam, Axial compressive behaviour of stub concrete-filled columns with elliptical stainless steel hollow sections, *Steel and Composite Structures*, 10 (6) (2010) 517-539.

[11] D. Lam, L. Gardner and M. Burdett, Axial compressive behaviour of stub concrete-filled columns with elliptical stainless steel hollow sections, *Advances in Structural Engineering*, 13 (3) (2010) 493-500.

[12] M. R. Bambach, Design of hollow and concrete filled steel and stainless steel tubular columns for transverse impact loads, *Thin-Walled Structures*, 49(10) (2011) 1251-1260.

[13] M. Yousuf, B. Uy, Z. Tao, A. Remennikov and J. Y. R. Liew, Impact behaviour of pre-compressed hollow and concrete filled mild and stainless steel columns, *Journal of Constructional Steel Research*, 96 (2014) 54-68.

[14] M. Yousuf, B. Uy, Z. Tao, A. Remennikov and J. Y. R. Liew, Transverse impact resistance of hollow and concrete filled stainless steel columns, *Journal of Constructional Steel Research*, 82 (2013) 177-189.

[15] L. H. Han, F. Chen, F. Y. Liao, Z. Tao and B. Uy, Fire performance of concrete filled stainless steel tubular columns, *Engineering Structures*, 56(2013) 165-181.

[16] Z. Tao, G. Mohamed, Heat transfer in concrete-filled carbon and stainless steel tubes exposed to fire, *Fire Safety Journal*, l61 (2013) 1-11.

[17] Z. Tao, G. Mohamed, T. Y. Song and L. H. Han, Experimental and numerical investigation of concrete-filled stainless steel columns exposed to fire, *Journal of Constructional Steel Research*, 118 (2016) 120-134.

[18] ABAQUS, *ABAQUS/Standard Version 6.14 User's Manual: Volumes* I-III (Dassault Systèmes Simulia Corp, Rhode Island, USA, 2014).

[19] EN 1992-1-2: 2004, *Design of concrete structures—Part 1-2: General rules—Structural fire design*, European committee for standardization, Brussels (2004).

[20] EN 1993-1-2: 2005, *Design of steel structures—Part 1-2: General rules—Structural fire design*, European committee for standardization, Brussels (2005).

[21] L. Gardner and K. T. Ng, Temperature development in structural stainless steel sections exposed to fire, *Fire Safety Journal*, 41 (2006) 185-203.

[22] J. Ghojel, Experimental and analytical technique for estimating interface thermal conductance in composite structural elements under simulated fire conditions, *Experimental Thermal and Fluid Science*, 28(4) (2004) 347-54.

[23] T. Y. Song, L. H. Han and H. X. Yu, Concrete filled steel tube stub columns under combined temperature and loading, *Journal of Constructional Steel Research*, 66 (3) (2010) 369-384.

[24] B. S. Zhang, and N. Bicanic, Residual fracture toughness of normal- and high-strength gravel concrete after heating to 600℃, *Materials Journal*, ACI 99 (3) (2002) 217-226.

[25] B. A. Izzuddin, A. Y. Elghazouli and X. Y. Tao. Realistic modeling of composite floor slabs under fire conditions, *Proceedings of the 15th ASCE Engineering Mechanics Conference*, New York, USA (2002).

[26] ISO 834-1, *Fire-resistance tests - elements of building construction - Part 1: General requirements*, International Standard ISO 834, Geneva (1999).

[27] L. H. Han, Q. H. Tan and T.Y. Song, Fire performance of steel reinforced concrete columns, *Journal of Structural Engineering*, ASCE 141(4) (2015) 04014128.

[28] L. H. Han, *Concrete filled steel tubular structures-theory and practice*, Science Press, Beijing, China (2016). (in Chinese)

[29] EN 1994-1-1: 2004, *Design of composite steel and concrete structures—Part 1-1: General rules and rules for buildings*, European committee for standardization, Brussels (2004).

[30] CECS 410: 2015, *Technical specification for stainless steel structures*, China Planning Press, Beijing (2015). (In Chinese)

[31] A. Espinos, M. L. Romero and D. Lam, Fire performance of innovative steel-concrete composite columns using high strength steels, *Thin-Walled Structures*, 106 (2016) 113-128.

Figure Captions

Fig. 1. Typical cross-sections of SRCFSST columns. (a) Circular section, (b) Rectangular section and (c) Square section.

Fig. 2. Meshing and boundary conditions of the FE model.

Fig. 3. Comparison between observed and predicted column failure modes. (a) C300-0.3 tested by Han et al. (2013) [15], (b) ST01 tested by Tao et al. (2016) [17] and (c) SRC2-1 tested by Han et al. (2015) [27].

Fig. 4. Comparison between tested and predicted fire resistances of CFSST and SRC columns.

Fig. 5. Temperature (T) versus time (t) curves of SRCFSST columns. (a) Concrete and (b) Profile.

Fig. 6. Typical failure mode of SRCFSST columns. (a) Stainless steel tube and (b) Carbon steel profile.

Fig. 7. Typical SRCFSST column axial deformation (Δ) versus time (t) curve.

Fig. 8. Proportion of load borne by each component of the SRCFSST column.

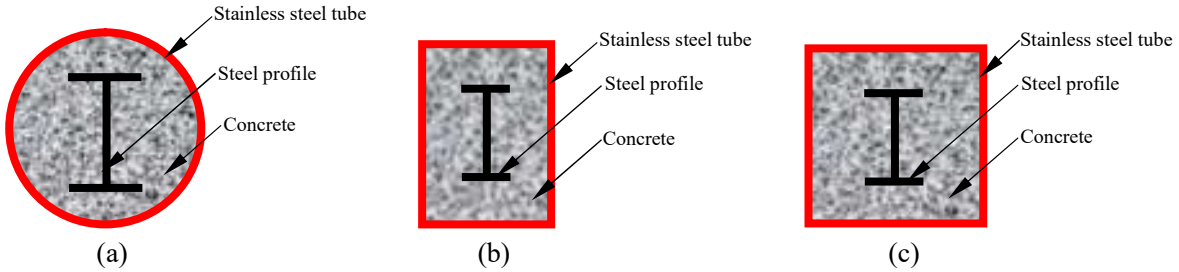


Fig. 1. Typical cross-sections of SRCFSST columns. (a) Circular section, (b) Rectangular section and (c) Square section.

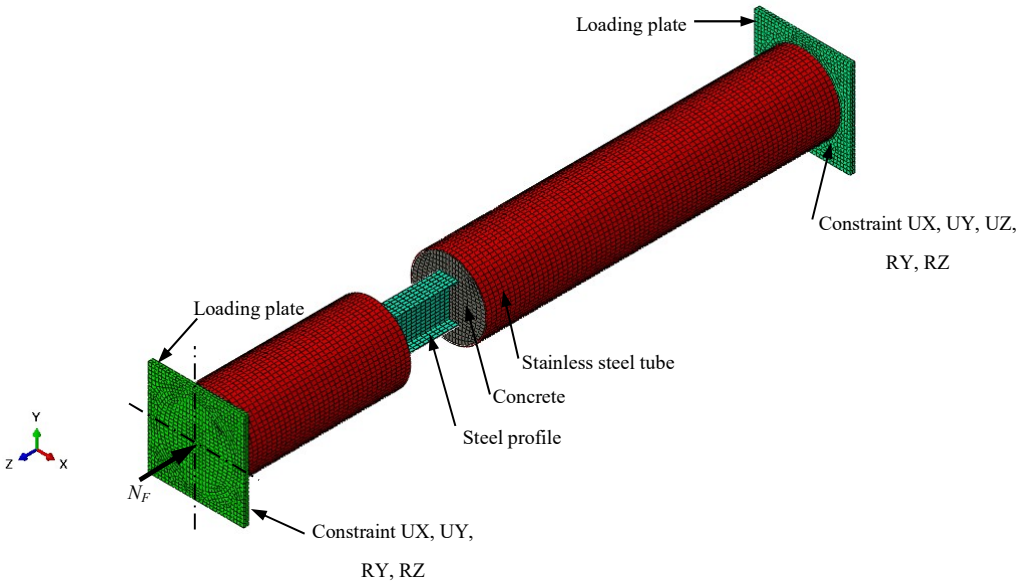
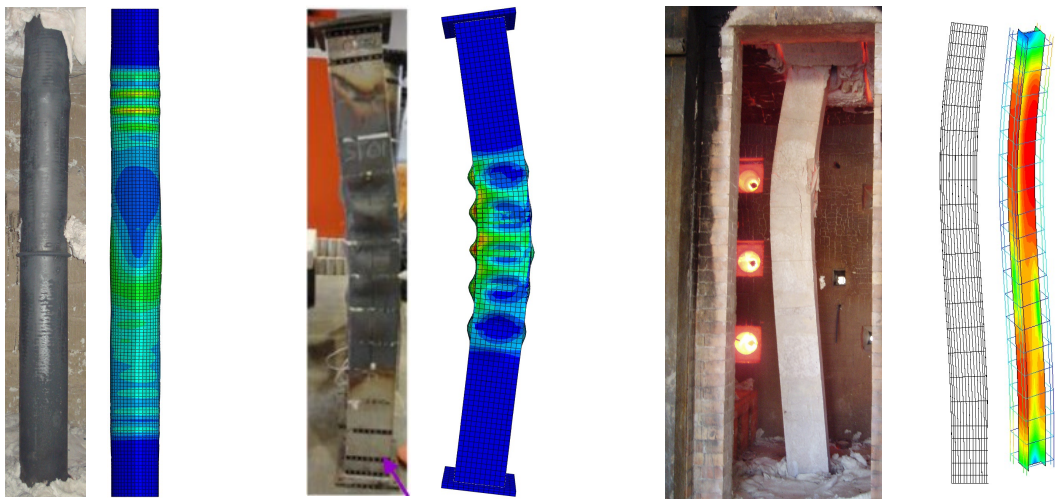


Fig. 2. Meshing and boundary conditions of the FE model.



(a) (b) (c)

Fig. 3. Comparison between observed and predicted column failure modes. (a) C300-0.3 tested by Han et al. (2013) [15], (b) ST01 tested by Tao et al. (2016) [17] and (c) SRC2-1 tested by Han et al. (2015) [27].

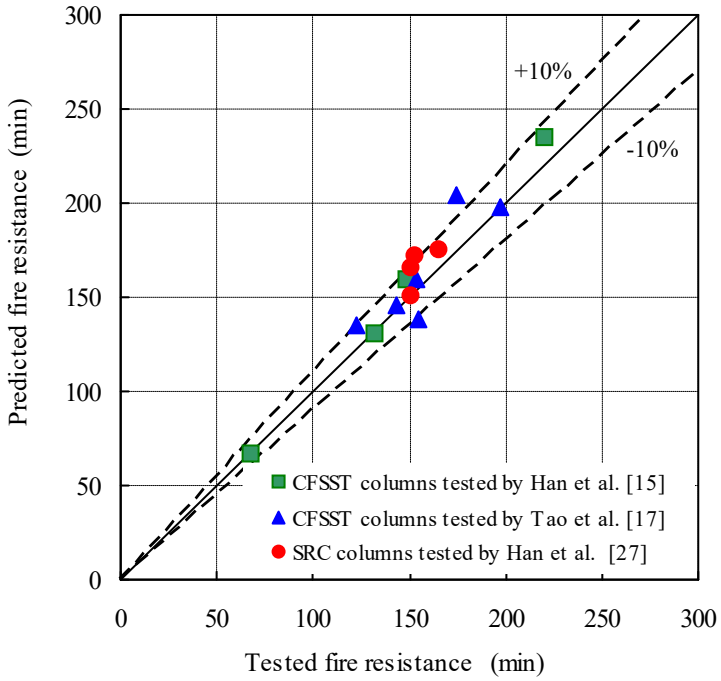
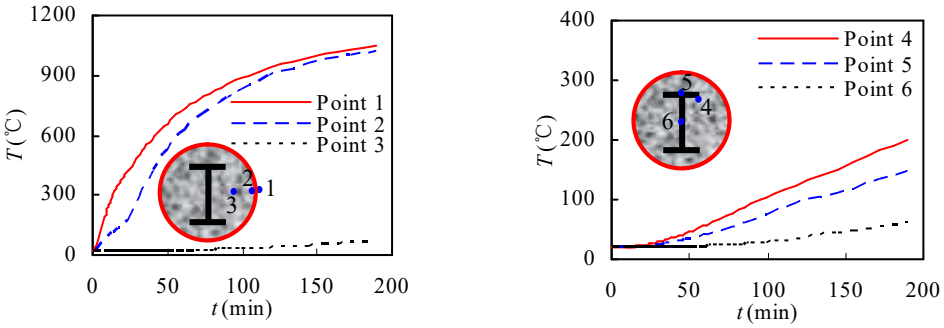
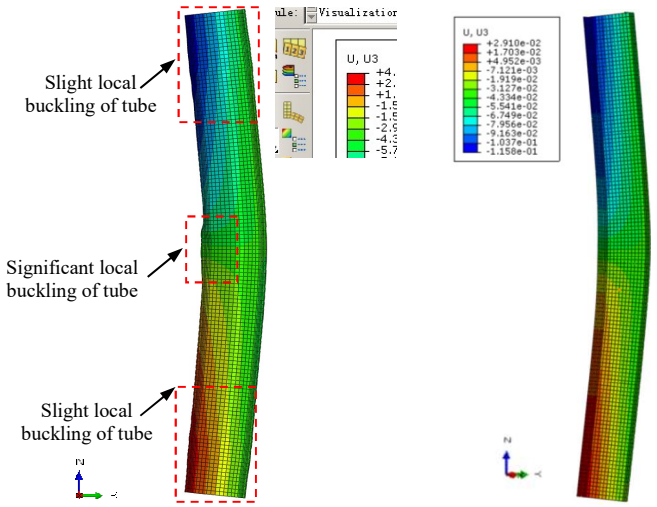


Fig. 4. Comparison between tested and predicted fire resistances of CFSST and SRC columns.



(a) (b)

Fig. 5. Temperature (T) versus time (t) curves of SRCFSST columns. (a) Concrete and (b) Profile.



(a) (b)

Fig. 6. Typical failure mode of SRCFSST columns. (a) Stainless steel tube and (b) Carbon steel profile.

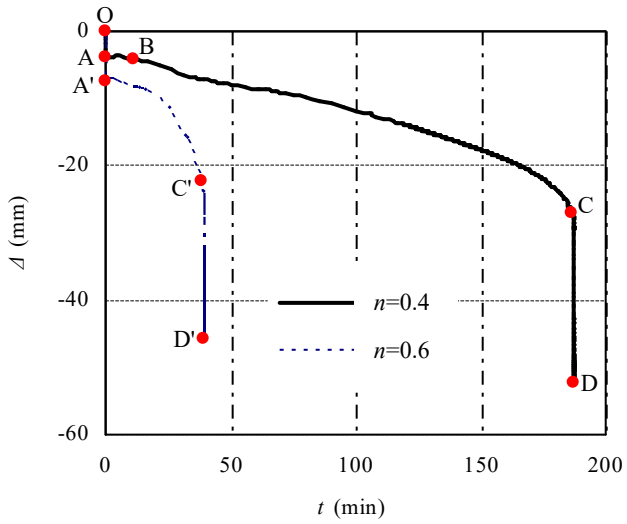


Fig. 7. Typical SRCFSST column axial deformation (Δ) versus time (t) curves.

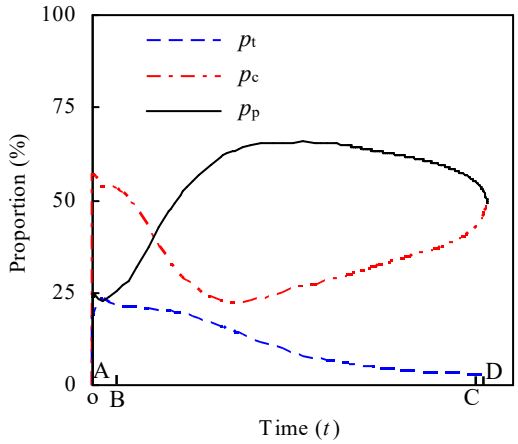


Fig. 8. Proportion of load borne by each component of the SRCFSST column.

Tables

Table 1. Geometrical and mechanical features of the composite columns with equal steel ratio (Series 1).

Table 2. Geometrical and mechanical features of the composite columns with equal load-bearing capacity (Series 2).

Table 1. Geometrical and mechanical features of the composite columns with equal steel ratio (Series 1).

Specimen	Dimension of tube (mm)	Diameter of concrete (mm)	Dimension of profiled steel (mm)	A_c (mm^2)	A_{sc} (mm^2)	A_{sp} (mm^2)	A_{ss} (mm^2)	A_{sp}/A_{ss} (A_{sp}/A_{sc})	Steel ratio (%)	N_u (kN)	Fire resistance (min)
CFST-16	800×16	768	--	4.6325×10^5	3.9408×10^4	--	--	0	8.51	4.12×10^4	41.5
CFSST-SR-16	800×16	768	--	4.6325×10^5	--	--	3.9408×10^4	0	8.51	3.43×10^4	64.8
SRCFSST-SR-14	796×14	768	400×200×6.4×6.4	4.6325×10^5	--	5014	3.4394×10^4	0.15	8.51	3.48×10^4	65.1
SRCFSST-SR-12	792×12	768	400×200×12.9×12.9	4.6325×10^5	--	1.0003×10^4	2.9405×10^4	0.34	8.51	3.51×10^4	69.2
SRCFSST-SR-10	788×10	768	400×200×19.7×19.7	4.6325×10^5	--	1.4966×10^4	2.4442×10^4	0.61	8.51	3.48×10^4	80.0
SRCFSST-SR-8	784×8	768	400×200×26.7×26.7	4.6325×10^5	--	1.9905×10^4	1.9503×10^4	1.02	8.51	3.56×10^4	102.9
SRCFSST-SR-6	780×6	768	400×200×33.9×33.9	4.6325×10^5	--	2.4818×10^4	1.4590×10^4	1.70	8.51	3.41×10^4	62.5

Note: For Specimen SRCFSST-SR-14, "SRCFSST" stands for the type of section; "SR" signifies for the series with equal steel ratio; "14" refers to the thickness (in mm) of the outer tube.

Table 2. Geometrical and mechanical features of the composite columns with equal load-bearing capacity (Series 2).

Specimen	Dimension of tube (mm)	Diameter of concrete (mm)	Dimension of profiled steel (mm)	A_c (mm^2)	A_{sc} (mm^2)	A_{sp} (mm^2)	A_{ss} (mm^2)	A_{sp}/A_{ss} (A_{sp}/A_{sc})	Steel ratio (%)	Fire resistance (min)
CFST-16	800×16	768	--	4.6325×10^5	3.9408×10^4	--	--	0	8.51	41.5
CFSST-LC-24	816.2×24.1	768	--	4.6325×10^5	--	--	5.9972×10^4	0	12.95	65.5
SRCFSST-LC-14	796×14	768	600×300×18.8×18.8	4.6325×10^5	--	2.1860×10^4	3.4394×10^4	0.64	12.14	119.1
SRCFSST-LC-12	792×12	768	600×300×22.5×22.5	4.6325×10^5	--	2.5935×10^4	2.9405×10^4	0.88	11.94	146.8
SRCFSST-LC-10	788×10	768	600×300×26.0×26.0	4.6325×10^5	--	2.9925×10^4	2.4442×10^4	1.22	11.74	187.4
SRCFSST-LC-8	784×8	768	600×300×29.6×29.6	4.6325×10^5	--	3.3830×10^4	1.9503×10^4	1.73	11.51	284.9
SRCFSST-LC-6	780×6	768	600×300×33.2×33.2	4.6325×10^5	--	3.7653×10^4	1.4590×10^4	2.58	11.28	71.9

Note: For Specimen SRCFSST-LC-14, "SRCFSST" stands for the type of section; "LC" signifies for the series with equal load-bearing capacity; "14" refers to the thickness (in mm) of the outer tube.